VI Apertureless Near-Field Optical Microscopy

In recent years, several types of apertureless near-field optical microscopes have been developed[1,2,3,4,5,6,7]. In such instruments, light scattered from or absorbed in the tip-sample region is detected. This signal depends on both: probe and sample, not only on sample features alone. For this kind of microscopy, it is favorable to use evanescent waves for excitation, in order to reject background light. In Fig. VI.1, a simple model of such a microscope is sketched.

One of the main components of the microscope is a glass prism. A plane wave incident from the glass side is reflected from the glass surface under an angle θ. If this angle exceeds the critical angle θ_c, total internal reflection occurs, and an evanescent wave is generated at the other side of the boundary, where an optically thinner medium is assumed. The evanescent wave is scattered and partly absorbed by particles on the surface, as well as by the probe tip. The latter is here idealized by a spherical silicon particle. The idealized tip scans the sample in a plane parallel to the surface at variable heights.

We have first calculated scan images of single Au- and Ag particles excited by evanescent waves. Their strong plasma resonances in the visible spectral range lead to interesting effects in the scan images (see Fig. VI.3). Fig. VI.2 shows wavelength-dependent cross sections for isolated small spherical Au- and Ag particles.

The maximums in the figures correspond to the dipolar plasma resonance of the particles. In the case of Au, the plasma frequency is strongly reduced by interband transitions. In real experiments, either the light scattered from the tip-sample region into a finite solid angle is detected by means of a microscope lens of given numerical aperture, or the absorption is detected, e.g. in a photo-acoustic

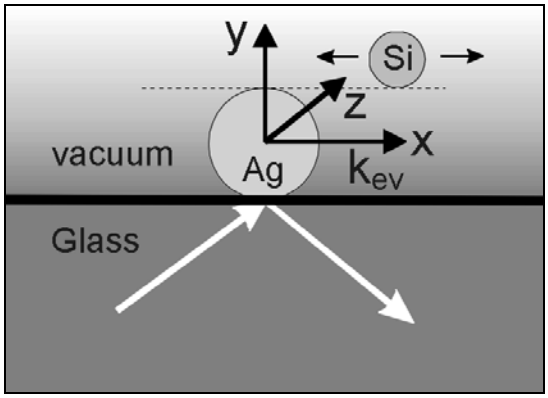

Fig. VI.1: Simplified model of an apertureless near-field optical microscope employing evanescent-wave excitation

experiment. In our initial calculations, we have determined only the total extinction and scattering cross sections. In principle, however, it is easy to include the effect of finite numerical aperture. For very small particles (ka<<1), the total extinction cross section is dominated by the absorption of

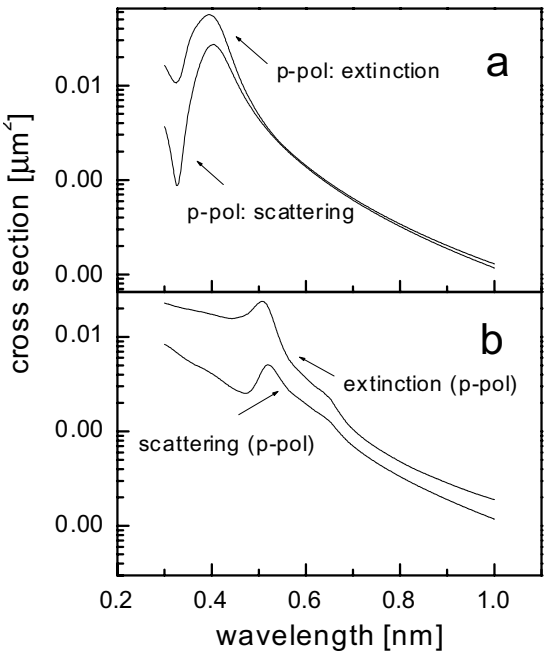

Fig. VI.2: Wavelength dependent scattering and extinction cross sections for small spherical particles (r=40 nm) of silver (**a**) and gold (**b**), respectively. Refractive index data from Palik

the silver particle, because the corresponding cross section is considerably larger than the scattering cross section. Here we have chosen a somewhat larger radius of the particle (a=40nm) to be detected (see Fig. VI.2).

Standard analysis restricts tip-sample interactions to dipole-dipole interactions. In the present chapter, aggregate Mie theory[8] is employed in order to self-consistently determine multipole coefficients of arbitrary order at the individual particles in the field of the exciting wave and to calculate from these coefficients total extinction and scattering cross sections. In our calculations, multiple scattering at the surface is neglected.

Fig. VI.3 shows the wavelength-dependent total scattering and extinction cross sections of a spherical silicon particle (r_1=20 nm) scanning over a single spherical silver particle (r=40 nm) at a height of $h=r_1+r_2$=60 nm above the center of the sample particle (Fig. VI.1). The respective signal is plotted in a grey scale figure as a function of the position of the scanning particle. Bright areas correspond to higher cross sections. The grey scales differ for each scan picture, such that black corresponds to the minimum value occurring within the scan range and white corresponds to the maximum value for the given wavelength and polarization. The right part of the figure represents the results of the dipole-dipole approximation. In the left part of the figure, multipoles up to order 9 are included in the calculation.

We first want to discuss the off–resonant case, which means the results for wavelengths far away from the plasma frequency and obtained within the dipole-dipole approximation (right part of Fig. VI.3), compare the image for λ=633nm. The images depend very much on the polarization of the evanescent wave. In all cases they are exactly mirror-symmetric with respect to the plane x=0. For off-resonant excitation, a second mirror plane y=0 exists to a very good approximation. In general, p-polarization yields much better images of the true object (the silver particle) than s-polarization. This is due to the rotation of the field in a p-polarized

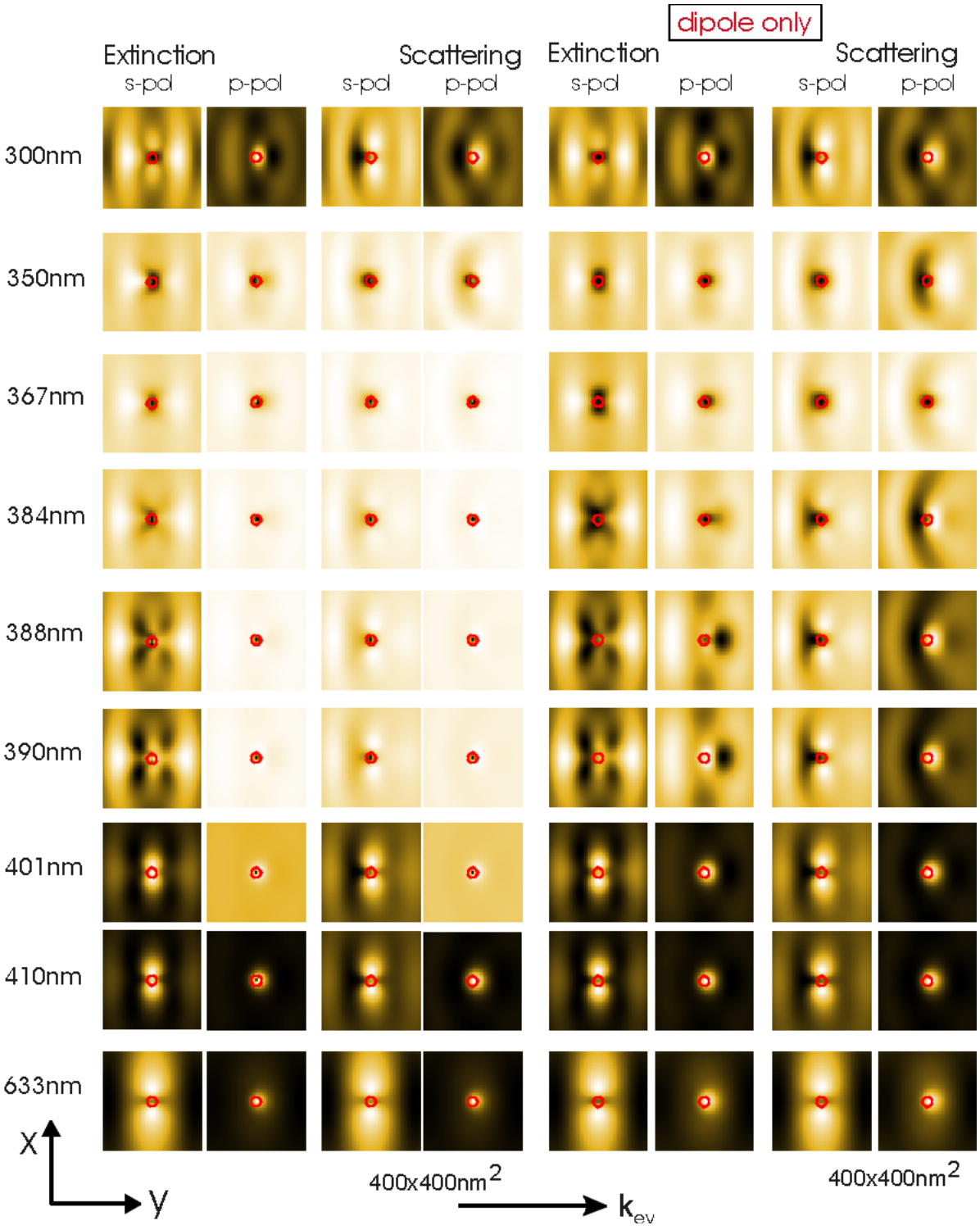

Fig. VI.3:
Left part: Apertureless SNOM images of a spherical Si-particle (r=20 nm) over a single silver particle (r=40 nm) at a height of (r=60 nm) above the center of the sample particle in dipole-dipole approximation. Dielectric constants taken from ref. 9.
Right part: Same scan images as in left part, but only the dipole is considered

evanescent wave, which results in a directional averaging, whereas in the case of s-polarization, the oscillation of the field in the y-direction leads to a strong dependence of the total cross sections on

the azimuthal position of the probe particle. It should be emphasized, that the scan images in Fig. VI.3 show the extinction and cross sections of two interacting particles depending on the position of the scanning particle. This is completely different from the angular characteristic of the light scattered by both particles. The comparison of off-resonant results obtained at different wavelengths (see results for 410 nm and 630 nm) shows that, as expected, the spatial resolution decreases for larger wavelengths. This result holds on, whether or not the retardation is neglected. Images obtained from extinction are very similar to those obtained from scattering. In the vicinity of the plasma frequency but still within the dipole-dipole approximation, the scan images become different for extinction and scattering and change rapidly, i. e. even for small wavelength steps. E.g. the comparison of the scan images obtained in scattering for the wavelengths 390 nm and 367 nm reveals the inversion of the contrast in the case of p-polarization and the loss of the mirror symmetry with respect to x=0.

In order to calculate the signal in the region of the contact with sufficient accuracy, higher multipole orders (n<=11) must be taken into account (see left part of Fig. VI.3). In Fig. VI.3, the scan images with the largest deviations between dipole-dipole approximation and the multipole calculations can be easily identified. For example, the extinction image for p-polarized excitation at a wavelength of 384 nm is clearly different in the vicinity of the contact point in comparison with the corresponding scan image obtained in dipole-dipole approximation. High spatial resolution in such an apertureless near-field optical microscope depends, of course, on the behavior of the respective signal in the vicinity of the contact point. The conclusion to be drawn from Fig. VI.3 is therefore, that high spatial resolution in apertureless SNOM is equivalent with the involvement of high- order multipoles, at least in the vicinity of the plasma resonances.

In order to discuss the contrast properties, Table VI.1 shows the maximum and minimum deviations of the cross sections from their mean values in the scan images. This determines the available signal in apertureless SNOM experiments of the respective particles at the given wavelengths. The background noise in such experiments should at least be an order magnitude below the given values. Normally, of course, modulation techniques will be used to suppress the background. This usually involves derivations of the scattered signal. The table indicates, that the contrast is better for p-polarized excitation, especially in the

Wave-length	Extinction				Scattering			
	p-pol		s-pol		p-pol		s-pol	
	mean value [W]	% varia-tion in image	mean value [W]	% varia-tion in image	mean value [W]	% varia-tion in image	mean value [W]	% varia-tion in image
300	2.62e-02	-2.06 +7.77	1.26e-02	-1.39 +1.51	5.08e-03	-9.79 +29.38	2.17e-03	-9.90 +7.43
367	8.87e-02	-21.51 +1.91	3.62e-02	-7.21 +1.87	4.68e-02	-45.51 +1.17	1.97e-02	-21.17 +1.57
388	1.03e-01	-31.22 +1.29	4.32e-02	-1.14 +1.05	5.95e-02	-56.85 +3.68	2.52e-02	-7.31 +1.14
633	1.99e-03	-5.19 +65.15	8.89e-04	-3.47 +8.22	1.52e-03	-6.56 +69.63	6.41e-04	-4.85 +10.52

Table VI.1 : Maximum and minimum deviations from the mean value of the cross sections for some selected scan images.

vicinity of the plasma frequency. E.g., at a wavelength of 388 nm, the lower deviation from the mean value of the cross section amount to more than 31% for this polarization, whereas the corresponding value for s-polarized excitation is only about 1%.

In addition to the calculations presented above, the material dependence of the scan images was examined.

Fig. VI.4 shows the power scattered or extinguished, respectively, from the incident evanescent wave for a scan over a spherical gold particle, whereas Fig. VI.5 shows the scan images of a sodium particle. Gold particles yield images, which are very similar to the off-resonant images of silver scans. The optical properties of gold cannot be described very

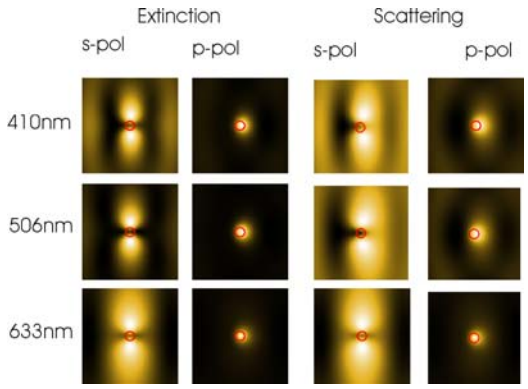

Fig. VI.4: Apertureless SNOM images of a gold particle. The geometric parameters are the same as in Fig. VI.2. Same scan area as in Fig. VI.3. Red circle: scattering spherical particle

well by the Drude model. But a rough estimate of the plasma frequency yields a

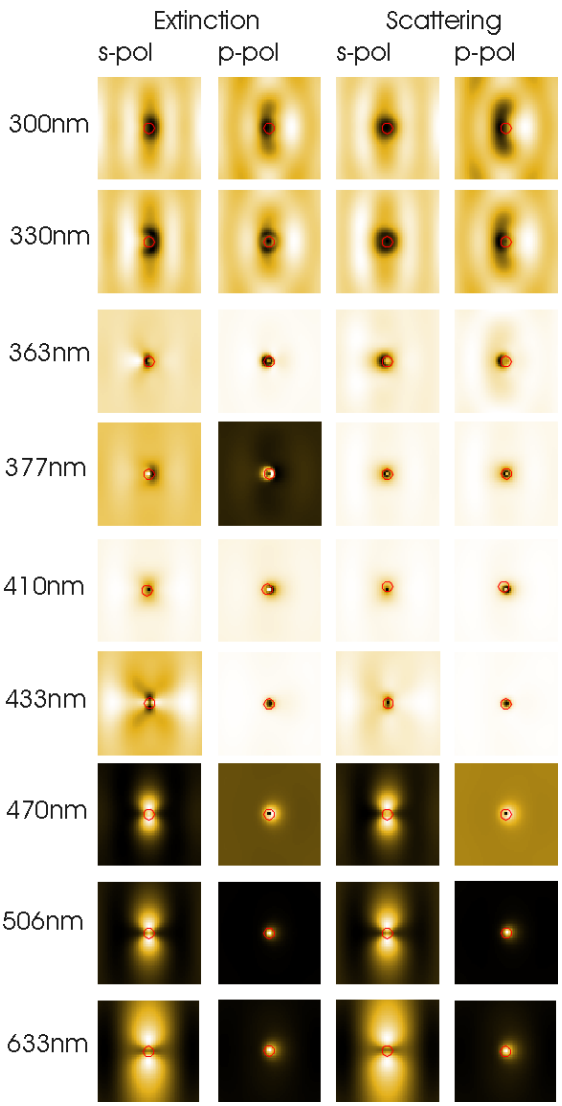

Fig. VI.5: Apertureless SNOM images of a sodium particle. The geometric parameters are the same as in Fig VI.2

very low value of about 150 nm. In order to analyze the scan images properly, separate multipole contributions to the corresponding single-particle cross sections have to be taken into account. Within the Drude model the multipolar resonances are determined by the plasma frequency.

In Fig. VI.6, the extinction cross sections of gold and sodium are shown. The corresponding scattering cross sections are not shown here, because they are similar to those obtained for the extinction. For gold, a spectrum dominated by a broad dipolar resonance is obtained, with a maximum at a wavelength of λ=506 nm. The higher multipoles are negligible. This fact and the large imaginary part of the dielectric function lead to simple image scans, shown above. Only exactly at the wavelength of the dipolar resonance, a slight deviation from the mirror symmetry with respect to z=0 is noticeable for the scattering scan image in the case of s-

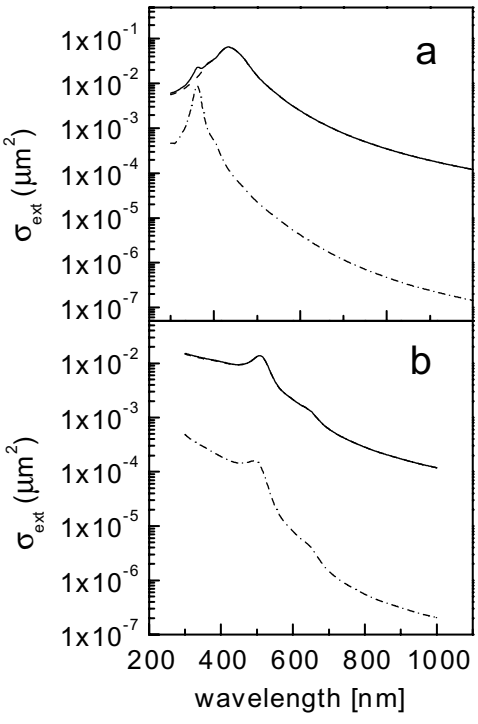

Fig. VI.6: Extinction cross sections for a spherical sodium (**a**) and a spherical gold particles (**b**), radii r = 40 nm. The total cross sections (solid lines) and the quadrupolar contributions (dashed lines) are shown, which contribute only in the case of sodium within a narrow wavelength range.

polarization.

Sodium, an alkali metal, can be described to a very good approximation by the Drude model. The plasma frequency is about 220 nm. The extinction cross section spectrum for a single sodium particle is dominated by the broad dipolar resonance at a wavelength of λ=433 nm but is, in contrast to gold, also influenced by the quadrupole, which exhibits a resonance at λ=363 nm. For the off-resonant case, far away from the plasma frequency (λ=470 nm, λ=506 nm and λ=633 nm), the scan images of the sodium particle are very similar to the off- resonant scan images of a silver particle. As for silver, the approach to smaller wavelengths is accompanied by a contrast inversion.

But here this effect already appears at a wavelength of about λ=430 nm, whereas for silver, the contrast inversion evolve for shorter wavelengths. At the wavelengths corresponding dipole (λ = 433 nm) and quadrupole (λ = 377 nm) resonances of the single sodium particle, the images have a complicated structure in the vicinity of the contact point. Very interesting is the contrast inversion, which occurs in the case of p-polarized excitation for the extinction image. This effect is caused by the phase properties of the interacting multipoles.

In Fig. VI.7, the scan over a dielectric spherical particle (SiO_2) is shown in order to underline, that many of the details in the previous paragraphs are caused by properties specific for metals.

Fig. VI.7 is similar to the non-resonant results obtained by scanning over a metallic particle. Because the particle is non-absorbing, the scattered and the extinguished power are equal and only the scattered power is shown. One difference is the minimum obtained in s-polarisation in the vicinity of the contact point, which is hardly visible, in contrast to metallic particles. In addition to that, the spatial resolution is much reduced, compared to scans over metallic particles.

The results demonstrate clearly the material dependence of the extinction and

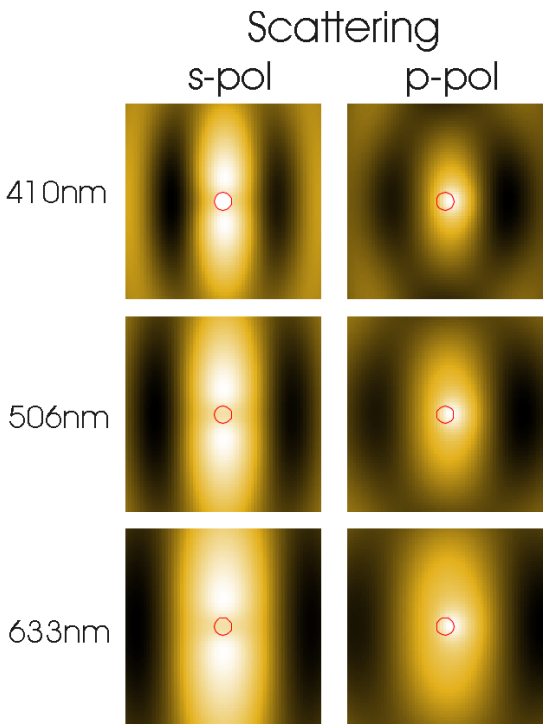

Fig. VI.7: Apertureless SNOM images obtained by scanning a Si particle across a SiO_2 particle. The geometric parameters are the same as in Fig. VI.3.

scattering cross sections in apertureless SNOM. This means, that in principle SNOM images allow to draw conclusions about the material properties of the examined sample. The previously described scan images of metallic particles were calculated under the assumption of two simplifications: the neglect of volume plasmons (see chapter II.1.2 and II.2.2.2) and of size-dependent corrections to the dielectric function[10]. The latter are caused by a reduction of the electron mean free path by surface scattering. This leads essentially to a spectral broadening of the resonances, which partly masks the strong wavelength-dependent effects discussed above. Therefore, these corrections have been deliberately omitted here. The first simplification can be made, because the scan images shown until now involved just one metallic particle. In this case, only negligible changes in the scan images occur due to the excitation of volume plasmons. The situation is completely different, if contacting metallic particles are present. In this case the local theory leads to unphysical non-converging cross sections (compare chapter V). In Fig. VI.8, the nonlocal wavelength-dependent cross sections of a cluster consisting of 4 contacting spherical metallic spheres (3 Ag- and 1 Au-particles) are shown. The maxima in the figures correspond to ,plasma resonances of the cluster. Thereby

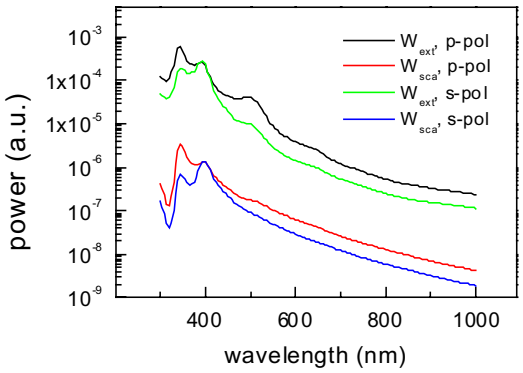

Fig. VI.8: Nonlocal scattering and extinction cross sections for a cluster of 4 metallic spherical particles (r=40 nm) consisting of three silver and one gold particle. Refractive index data from Palik

the resonance at around 500 nm is caused by the gold particle, and the other two resonances at shorter wavelengths are related to the silver particles.

Fig. VI.9 shows images obtained by a scan of the Au-particle over the 3 contacting Ag-particles with radii of 5 nm. All images were calculated with a maximum order, which is listed in the figure.

As mentioned above and described in detail in chapter V, the local theory does not lead to converging results. When the maximum multipolar order is increased by one, even contrast reversals are obtained. In contrast to the local theory, the nonlocal images are rapidly converging as a function of the maximum order (compare chapter V). The required order for convergence, however, depends on the wavelength. For a wavelength λ= 460nm,

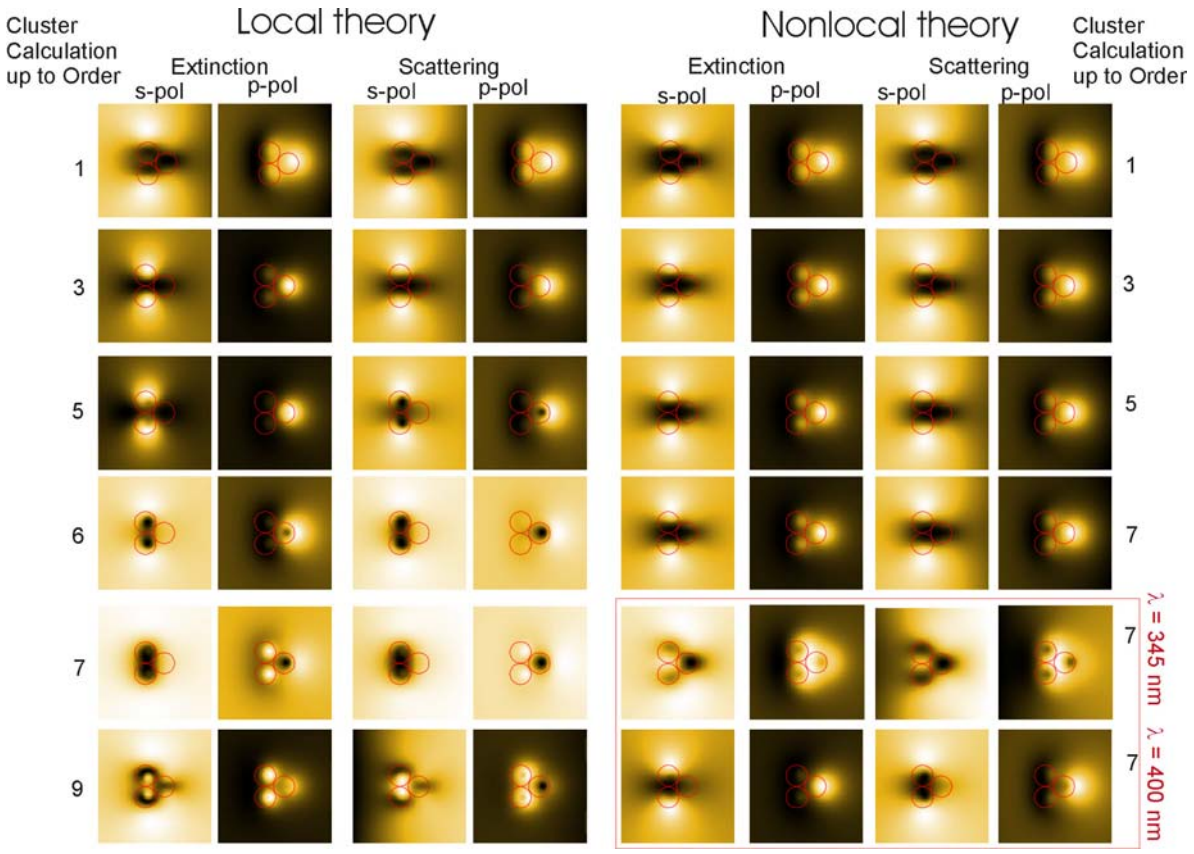

Fig. VI.9: Apertureless SNOM images obtained by a scan of a gold particle (a=5nm) over a cluster of three spherical silver particles (a=5nm), in the field of an evanescent wave, λ= 460nm (and right sight last row: λ= λ= 400nm), generated by total internal reflection at the surface of a glass prism (n=1.5).

multipole order 3, which are similar to the dipolar results of the local theory. In general, however, higher orders are required. For a wavelength of λ= 400nm images are obtained, which differ from those obtained at 460 nm, in that, for p-polarisation, the two particles on the left are hardly visible any more. In contrast to this, at a wavelength of 345 nm, all 3 particles can be seen in the scattering image even for s-polarisation. In the case of p-polarisation a contrast inversion occurs within the two particles on the left compared to the results obtained at 400nm.

A comparison of the results discussed in the present chapter with experimental work is, of course, desirable. Apertureless SNOM images of isolated colloidal silver or gold particles or well-defined clusters of such particles have, however, not been reported in the literature. Moreover, very few experimental data are available in the blue or near UV spectral range, where plasmonic resonances of those particles occur. In two recently published papers, randomly distributed clusters[11] and metal island clusters[12] were investigated. Strong fluctuations of the local near-field were

found in ref. 11 and ascribed to Anderson localization of plasmonic surface excitations. These findings can, of course, not be compared with our results. The corresponding results cannot be compared with our results. Theoretical investigations of apertureless SNOM images were recently published by Quinten.[13] He confined his work to the local theory and only multipole orders up to order 3 were considered. It was shown above (Fig. VI.9), that such calculations are not meaningful.

References

[1] F. Zenhausern, M. P. O' Boyle, H. K. Wickramasinghe, Appl. Phys. Lett. **65**, 13 (1994)
[2] F. Zenhausern, Y. Martin H. K. Wickramasinghe, Science **269**, 1083 (1995)
[3] Y. Martin, F. Zenhausen, H. K. Wickramasinghe, Appl. Phys. Lett. **68**, 18 (1996)
[4] M.Labardi Patane,Allegrini, Appl. Phys. Lett. **77**, 5 (2000)
[5] S. Kawata, Y. Inouye, Ultramicr. **57**, 313 (1995)
[6] R. Bachelot, P. Gleyzes, A. C. Boccara, Appl. Opt. **36**, 2160 (1997)
[7] G. Wurtz, R. Bachelot, P. Royer, Rev. Sci. Instr. **69**, 1735 (1998)
[8] Gérardy & Ausloos, Phys. Rev. B **25**, 13 (1982)
[9] D. Palik, *Handbook of Optical Constants of Solids,* (Academic Press, New York, 1985)
[10] H. Kreibig, M. Vollmer, *Optical Properties of Metal Clusters*, Springer Series in Material Science **25** (Springer Verlag, Berlin, 1995)
[11] S Gresillon, L. Aigouy, A. C. Boccara, J. C. Rivoal, Phys. Rev. Lett. **82**, 4520 (1999)
[12] S. Gresillon, S. Ducourtiex, A. Lahrech, L. Aigouy, J. C. Rivol, A. C. Boccara, Appl. Surf. Sc. **164**, 118 (2000)
[13] M. Quinten, Appl. Phys. B **70**, 579 (2000)